Rapid magma evolution constrained by zircon petrochronology and ^{40}Ar/^{39}Ar sanidine ages for the Huckleberry Ridge Tuff, Yellowstone, USA

Tiffany A. Rivera[1,2], Mark D. Schmitz[2], James L. Crowley[2], and Michael Storey[1]
[1]Quaternary Dating Laboratory, Roskilde University, Universitetsvej 1, 4000 Roskilde, Denmark
[2]Department of Geosciences, Boise State University, 1910 University Drive, Boise, Idaho 83725, USA

ABSTRACT

Understanding the time scales of magmatic differentiation, storage, and eruption of large-volume silicic magmas is a primary goal of igneous petrology. Within the Huckleberry Ridge Tuff (HRT; Idaho, USA), representing the earliest and largest caldera-forming eruption associated with Yellowstone volcanic activity, zircon morphological zoning patterns coupled to strongly correlated changes in Ti-in-zircon thermometry and trace element indicators of progressive differentiation provide a proxy record for the evolution of the HRT member B magma body. Tandem in situ and isotope dilution U-Pb dating of single zircon crystals demonstrates an absence of pre-Pleistocene xenocrysts, but reveals the presence of antecrysts recycled from pre-caldera rhyolites in the HRT magma. The petrochronologic interpretation of autocrystic zircon thermal, chemical, and temporal characteristics suggests that HRT member B differentiated over ~10 k.y. prior to eruption at 2.0794 ± 0.0046 Ma as defined by new astronomically calibrated, single-crystal total fusion ^{40}Ar/^{39}Ar sanidine analyses. This refined eruption age demonstrates that the transitional polarity preserved by HRT member B does not record the Reunion subchron, but rather a separate, younger geomagnetic event. Our novel approach places the thermal and chemical regime of silicic magmas within a temporal context and demonstrates the rapid evolution of a large volume of silicic magma.

INTRODUCTION

The Yellowstone volcanic field (Wyoming, Idaho, and Montana, USA) is one of the best studied sources of super-eruptions. Situated at the eastern terminus of the Snake River Plain, the source of volcanism has been linked to a stationary mantle plume beneath the continental lithosphere (e.g., Pierce and Morgan, 2009), upwelling mantle as a result of Farallon slab displacement (James et al., 2011), or propagating small-scale convection in the upper mantle (Humphreys et al., 2000). The earliest caldera-forming Pleistocene ignimbrite in the Yellowstone region is the Huckleberry Ridge Tuff (HRT), which is divided into three welded tuff units (members A, B, and C) with an estimated volume of >2500 km^3 (Christiansen and Blank, 1972; Obradovich, 1992). A paleomagnetic study of the members revealed intermediate magnetic directions (Reynolds, 1977), signifying deposition during a period of transitional geomagnetic polarity historically associated with the Reunion normal polarity subchron.

Recalculations of high-precision ca. 2.1 Ma ^{40}Ar/^{39}Ar dates for the HRT member B to the same Fish Canyon Tuff sanidine (FCTS) monitor value (Kuiper et al., 2008; Lanphere et al., 2002; Ellis et al., 2012) give conflicting eruption ages, resulting in two interpretations of the Pleistocene geomagnetic polarity time scale (Fig. 1). Ellis et al. (2012) determined a temporal offset between the eruption of HRT member C and the ages for members A and B, suggesting that member C erupted during a period

of reversed polarity (C2r.1r), while members A and B were deposited during the Reunion subchron. Although Gansecki et al. (1998) determined a slightly younger, less-precise age for HRT member B, they made an essential observation overlooked by subsequent studies. Single-crystal sanidine fusion experiments produced a tail of older ages attributed to roofward or sidewall cannibalization of previously crystallized material preceding eruption, a conclusion anticipating the recognition of antecrystic contributions to the cargo load of intermediate to silicic magma systems (Miller et al., 2007).

This contribution seeks to resolve the age of the HRT member B crystal cargo, its eruption, and the associated geomagnetic polarity excursion using a multichronometric approach, including the tandem use of zircon trace element chemistry, Ti-in-zircon thermometry, and ^{238}U/^{206}Pb dating, along with an astronomically calibrated ^{40}Ar/^{39}Ar sanidine age. Our petrochronology defines autocrystic and antecrystic components of the zircon cargo, allowing an interpretation of crystallization and eruptive time scales. The resulting ^{238}U/^{206}Pb zircon and ^{40}Ar/^{39}Ar sanidine ages suggest that the HRT records a separate polarity excursion distinctly younger than the Reunion subchron.

METHODS

Single-crystal ^{40}Ar/^{39}Ar HRT member B sanidine fusion experiments were measured relative to the astronomically calibrated A1 tephra sanidine (A1TS; 6.943 ± 0.005 Ma equivalent to

FCTS of 28.172 ± 0.028 Ma; Rivera et al., 2011). Argon isotopic analyses were performed on a Noblesse multicollector mass spectrometer at the QUADLAB (Quaternary Dating Laboratory, Roskilde University, Denmark) following procedures similar to those of Brumm et al. (2010) and Rivera et al. (2011). Zircon cathodoluminescence (CL) imaging, trace element analyses by laser ablation–inductively coupled plasma–mass spectrometry (LA-ICPMS), Ti-in-zircon thermometry calculations (Ferry and Watson, 2007), and chemical abrasion–thermal ionization mass spectrometry (CA-TIMS) age determinations follow the methodology described in Rivera et al. (2013). Additional details and data are available in the GSA Data Repository[1].

RESULTS

^{40}Ar/^{39}Ar Sanidine Geochronology

HRT member B sanidine analyses define a multimodal distribution characterized by a major asymmetric mode and minor tail to older ages, with a weighted mean date of 2.0857 ± 0.0028/0.0046 Ma (n = 64; mean square of weighted deviates, MSWD = 3.99; Fig. 1). All uncertainties are reported as 2σ analytical error (/systematic error) unless otherwise stated. ^{40}Ar/^{39}Ar age uncertainties include the error on the neutron flux parameter (J). To address the asymmetric distribution, we explored a mixture modeling approach (Sambridge and Compston, 1994) to deconvolve two overlapping normal distributions. The youngest mode (n = 47) yields a weighted mean date of 2.0772 ± 0.0030/0.0046 Ma, while the older mode has a date of 2.0971 ± 0.0032/0.0046 Ma (n = 17). The tail to older dates includes a minor peak (n = 3) at 2.1298 ± 0.0048 Ma and additional single crystal dates extending to 2.27 Ma. The results presented here were determined relative to the A1TS monitor (Rivera et al., 2011), but the date of the youngest mode relative to FCTS of 28.201 Ma is 2.0794 ± 0.0030/0.0046 Ma, which we use throughout the text for simplicity in comparing ^{40}Ar/^{39}Ar dates from multiple publications.

Figure 1. A: Age-probability distribution and percent ⁴⁰Ar* plot (1σ analytical uncertainty; outliers shown as open symbols); calculated ages are shown with 2σ analytical uncertainty. B: Proposed ages for Reunion (Feni Drift) and Huckleberry Ridge Tuff (HRT) polarity chrons with published sanidine and zircon ages. ⁴⁰Ar/³⁹Ar ages recalculated to Fish Canyon Tuff sanidine age of 28.201 Ma (Kuiper et al., 2008). GTS2012—Gradstein et al. (2012); S14—Singer (2014).
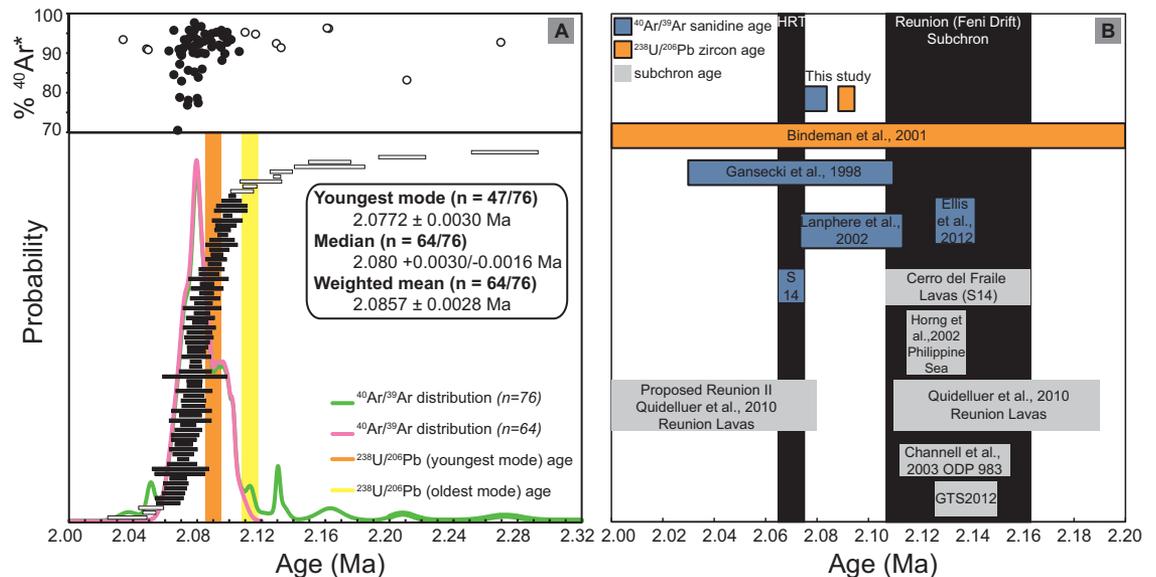
Zircon Trace Elements and Ti-in-Zircon Thermometry

Three chemical domains correlated to discernible ranges of Ti-in-zircon crystallization temperatures are defined by LA-ICP-MS spot analyses (n = 90) on 67 HRT member B zircon crystals. Chemical domain 1 (CD1) consists of high-temperature ($T > 800$ °C) analyses within relatively CL-homogeneous central areas of elongate prismatic crystals. High-T analyses trend toward higher Eu/Eu* values (Fig. 2), lower concentrations of incompatible trace elements (ITEs; e.g., Nb, Th, and U), a shallow slope of heavy rare earth elements (HREEs), and low Th/Y. Chemical domain 3 (CD3) consists of low-T (<750 °C) analyses from relatively luminescent, weakly oscillatory zoned domains that trend toward lower Eu/Eu* values, higher ITE concentrations, and a steeper slope of HREEs. Both apparent core and rim analyses compose this group. The mid-temperature (750–800 °C) group composing chemical domain 2 (CD2) has concentrations and ratios intermediate between CD1 and CD3, and consists predominantly of core analyses. The steepening of HREEs, depletion in Y + REE, suppression of Th compared to U, and increase in Th/Y are consistent with the crystallization of Th + light REE–rich chevkinite in the HRT member B magma (Christiansen, 2001).

The superposition of temperature and chemical domains within single crystals is consistent with down-temperature crystallization. Low-T CD3 rim analyses are often paired with higher T CD1 cores; temperatures can vary as much as 100 °C between the core and rims of individual crystals (Fig. 2). No high-T CD1 or CD2 rims were found, or any core paired with a rim of higher temperature outside of the ±10 °C uncertainty on Ti-in-zircon temperatures (Rivera

et al., 2013). Higher CD1 temperatures are consistent with zircon saturation temperatures for Yellowstone tuffs (830–910 °C) and inferences of zircon as a near-liquidus phase (Bindeman et al., 2001). Cooler CD3 temperatures are consistent with eruption temperatures determined by Ti-in-quartz thermometry for young, high-volume silicic magmas of the Yellowstone region (Vazquez et al., 2009).

Zircon crystals extracted from the underlying Snake River Butte (SRB) rhyolite flow (e.g., Christiansen, 2001) exhibit morphological, chemical, and thermal patterns similar to HRT member B. In particular, low-T domains in both samples are nearly identical in temperature and geochemical ranges and trends. The two samples contrast in that high-T analyses of SRB are slightly hotter (~850–900 °C) with smaller Eu anomalies, higher ITE concentrations, and steeper HREE slopes than CD1 analyses of HRT member B.

CA-TIMS U/Pb Age Determinations

HRT member B zircon crystals (n = 23) spanning the compositional and thermal range yield a multimodal distribution of ²³⁸U/²⁰⁶Pb dates ranging from 2.2064 ± 0.0133 Ma to 2.0859 ± 0.0066 Ma (Fig. 2). Excluding four crystals older than 2.13 Ma, the data plot into two overlapping but resolvable modes. Using a 95% confidence interval outlier rejection criteria, the youngest mode yields a weighted mean of 2.0915 ± 0.0034/0.0042 Ma (n = 13, MSWD = 0.91), and an older mode (n = 6) has a weighted mean of 2.1142 ± 0.0043/0.0050 Ma. Alternatively, mixture modeling deconvolution yields ages of 2.0912 ± 0.0037 Ma and 2.1129 ± 0.0048 Ma for the two modes. SRB zircon crystals are consistently older than HRT member B, with dates ranging from 2.241 ± 0.040 Ma to 2.163 ±

0.014 Ma (n = 9; Fig. 2). The youngest mode (n = 4) yields a weighted mean date of 2.1724 ± 0.0064/0.0069 Ma.

DISCUSSION

Zircon Petrochronology

Combining radioisotopic dating with CL imaging, thermometry, and trace element compositions aids in determining when zircon crystallized with respect to the production, differentiation, and eruption of its host magma. Key to this effort is the Ti-in-zircon thermometer (Ferry and Watson, 2007), which may allow a direct linking of zircon crystallization temperature to the coexisting melt composition and timing of crystallization from trace element and U-Pb ratios recorded in the same grain. Although it has been suggested that Ti partitioning may be partly facilitated by nonequilibrium effects other than temperature (Fu et al., 2008; Hofmann et al., 2009), our observations support the fidelity of the thermometer (Watson and Harrison, 2005; Claiborne et al., 2010) in that we extract consistent correlations of Ti-in-zircon temperatures with a variety of trace element concentrations and ratios predicted by down-temperature crystallization and differentiation. Variation within and among the HRT member B zircon chemical domains can be quantified using fractional crystallization modeling of the differentiation index Eu/Eu*, which predicts the increasing negative anomaly of the CD1 and CD2 groups after 10%–20% sanidine crystallization across Ti-in-zircon temperatures (750–850 °C). An additional 10%–20% of eutectic crystallization of sanidine, quartz, and plagioclase is required to produce the decreasing Eu/Eu* of CD3 zircon rims from 750 to 700 °C. Thus the entire chemical and thermal regime recorded in 150 °C of differentiation corresponds to ≤40% crystallinity. These
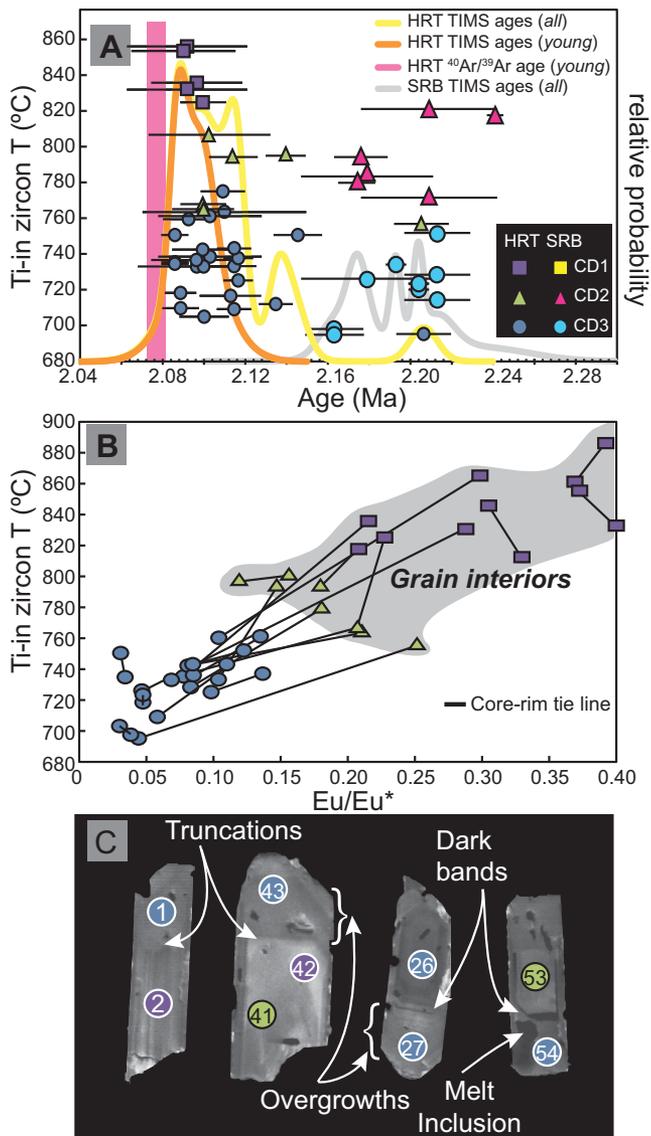
Figure 2. A: Temperature versus $^{238}U/^{206}Pb$ age. SRB—Snake River Butte; HRT—Huckleberry Ridge Tuff; TIMS—thermal ionization mass spectrometry. B: Temperature versus Eu anomaly. C: Cathodoluminescence images of HRT zircon grains with morphological features and laser ablation–inductively coupled plasma–mass spectrometry spot coded by chemical domain.

correlations between temperature, trace element concentration, and degree of magmatic differentiation provide a means of assigning petrologic significance to the high-precision CA-TIMS analyses on the same crystals.

Origins of the Zircon Crystal Load

Xenocrystic cores of Pliocene or older age are absent within the HRT member B crystal cargo; such domains would have been resolved in LA-ICP-MS analyses of targeted cores identified in CL images. This is consistent with derivation of HRT magmas in a deep crustal source region at temperatures above Zr saturation, leading to dissolution of potentially xenocrystic zircon crystals in the early stages of melt extraction. Autocrystic grains are those composing the youngest, dominant mode of the $^{238}U/^{206}Pb$ dates, a mode that spans the entire core to rim thermal and chemical crystallization spectrum and may capture the full differentiation history of the HRT magma. Thus, time scales of HRT

magma generation, storage, and differentiation (from melt generation to ~40% crystallization) were quite rapid (≤10 k.y.). Alternatively, all grains ranging from 2.086 to 2.117 Ma may represent stages of magmatic evolution. Earlier formed, lower *T* grains could have crystallized along the cooling and solidifying sides and roof of the nascent magma chamber, offering nuclei for subsequent rim overgrowth to occur either in situ or during later remobilization of marginal crystal accumulations. Remobilization could be recorded by the 2.092 Ma crystal mode through the larger range of Ti-in-zircon temperatures and related indices of magma differentiation. During remobilization, influx of a hotter, less-evolved magma must have occurred, as evidenced by the youngest grains with CD1 cores and CD3 rims with increasing negative Eu anomalies and ITE concentrations from core to rim. In this scenario, the time scales of magma generation, storage, and differentiation were somewhat longer, yet still rapid, on the order of ≤40 k.y.

Alternatively, the subgroup of crystals with $^{238}U/^{206}Pb$ ages slightly older than the youngest mode could represent scavenged antecrysts, or composite crystals with antecrystic cores and autocrystic rims. Most of these crystals have complexly and/or strongly zoned internal domains often separated from overgrown, luminescent, weakly zoned rims by a thin CL-dark zone (Fig. 2). Rims of these crystals share chemical similarities with CD3 zircon, but cores have diverse CD2 and CD3-like compositions. In some cases, these compositions are clearly anomalous and not in equilibrium with the same HRT magma composition as the majority of the crystal load. Within this interpretation, antecrystic core components must be at least 25–120 k.y. older than the autocrystic portion of the crystal cargo, given that CA-TIMS analyses average age variations in composite grains. We hypothesized that lavas like the SRB rhyolite, or unerupted intrusive bodies (Christiansen, 2001), were likely contributors to the antecrystic cargo. Our petrochronology of the SRB rhyolite provides strong support for this hypothesis, both in the similar geochemistry of the zircons and the ~80 k.y. older age of the SRB rhyolite with respect to HRT member B. In summary, we strongly favor the hypothesis that the oldest HRT member B zircons are composite crystals with antecrystic SRB zircon cores surrounded by autocrystic HRT member B zircon rims.

The preference for an antecrystic origin to describe the asymmetric distribution of zircon CA-TIMS ages is supported by the $^{40}Ar/^{39}Ar$ geochronology. Sanidine dates obtained in this study, similar to the results of Gansecki et al. (1998), show a spread beyond that expected from analytical considerations, including a mode of crystals ~20 k.y. older than the autocrystic mode, as well as a tail of dates older than 2.135 Ma. Due to the kinetics of Ar diffusion in sanidine, these older crystals are most likely antecrysts incorporated into the HRT magma no more than months to years before eruption. Gansecki et al. (1998) interpreted such older crystals as roofward or sidewall cannibalization of previously crystallized cognate material; we posit that these crystals could also be entrained from slightly older igneous rocks comminuted during the climactic eruption. If the same mechanism applies across the HRT crystal load, sanidine captures the last aliquot of antecrystic recycling, whereas zircon records entrainment in composite crystal cores throughout the aggregation of the HRT magma. We thus favor the antecrystic origin for older sanidine and zircon dates, and the rapid aggregation and differentiation of the HRT magma ~10 k.y. prior to eruption at 2.0794 ± 0.0046 Ma.

Implications for the Geomagnetic Polarity Time Scale

The transitional polarity of the HRT has been attributed to several different geomagnetic

polarity events, most often a relationship to the Reunion subchron (e.g., Obradovich, 1992). $^{40}Ar/^{39}Ar$ sanidine data obtained by Ellis et al. (2012) suggest eruption of HRT member B at ca. 2.134 Ma, consistent with proposed ages for the subchron (Fig. 1). However, the youngest mode of $^{238}U/^{206}Pb$ zircon dates obtained in our study suggests zircon crystallization as recently as 2.092 Ma, with eruption at 2.079 Ma as indicated by the youngest and main distribution of $^{40}Ar/^{39}Ar$ sanidine ages. The discrepancy between our ages and that of Ellis et al. (2012) cannot be accounted for by the choice and age of neutron flux monitor, and it is not geologically plausible for sanidine to record ages older than zircon in the same volcanic deposit. Placement of the HRT member B eruption within the Reunion subchron (Ellis et al., 2012) does not account for the transitional polarity preserved within the eruptive unit (Reynolds, 1977). New $^{40}Ar/^{39}Ar$ data from Cerro del Fraile (Fig. 1) and HRT member B suggest that the termination of the Reunion (Feni Drift) subchron occurred ~40 k.y. prior to the eruption of HRT member B (Singer, 2014). Following Lanphere et al. (2002) and Singer (2014), our work supports their observations that the eruption of HRT member B did not occur within and is not associated with the Reunion subchron, but instead preserves the transitional polarity related to a separate geomagnetic excursion.

REFERENCES CITED

Bindeman, I., Valley, J., Wooden, J., and Persing, H., 2001, Post-caldera volcanism: In situ measurement of U-Pb age and oxygen isotope ratio in Pleistocene zircons from Yellowstone caldera: Earth and Planetary Science Letters, v. 189, p. 197–206, doi:10.1016/S0012-821X(01)00358-2.

Brumm, A., Jensen, G.M., van den Bergh, G.D., Morwood, M.J., Kurniawan, I., Aziz, F., and Storey, M., 2010, Hominins on Flores, Indonesia, by one million years ago: Nature, v. 464, p. 748–752, doi:10.1038/nature08844.

Channell, J.E.T., Labs, J., and Raymo, M.E., 2003, The Reunion subchronozone at ODP Site 981 (Feni Drift, North Atlantic): Earth and Planetary Science Letters, v. 215, p. 1–12, doi:10.1016/S0012-821X(03)00435-7.

Christiansen, R.L., 2001, Geology of Yellowstone National Park: The Quaternary and Pliocene Yellowstone Plateau volcanic field of Wyoming, Idaho, and Montana: U.S. Geological Survey Professional Paper 729-G, 145 p.

Christiansen, R.L., and Blank, H.R.J., 1972, Volcanic stratigraphy of the Quaternary Rhyolite Plateau in Yellowstone National Park: U.S. Geological Survey Professional Paper 729-B, 18 p.

Claiborne, L.L., Miller, C.F., and Wooden, J.L., 2010, Trace element composition of igneous zircon: A thermal and compositional record of the accumulation and evolution of a large silicic batholith, Spirit Mountain, Nevada: Contributions to Mineralogy and Petrology, v. 160, p. 511–531, doi:10.1007/s00410-010-0491-5.

Ellis, B.S., Mark, D.F., Pritchard, C.J., and Wolff, J.A., 2012, Temporal dissection of the Huckleberry Ridge Tuff using the $^{40}Ar/^{39}Ar$ dating technique: Quaternary Geochronology, v. 9, p. 34–41, doi:10.1016/j.quageo.2012.01.006.

Ferry, J.M., and Watson, E.B., 2007, New thermodynamic models and revised calibrations for the Ti-in-zircon and Zr-in-rutile thermometers: Contributions to Mineralogy and Petrology, v. 154, p. 429–437, doi:10.1007/s00410-007-0201-0.

Fu, B., Page, F.Z., Cavosie, A.J., Fournelle, J., Kita, N.T., Lackey, J.S., Wilde, S.A., and Valley, J.W., 2008, Ti-in-zircon thermometry: Applications and limitations: Contributions to Mineralogy and Petrology, v. 156, p. 197–215, doi:10.1007/s00410-008-0281-5.

Gansecki, C.A., Mahood, G.A., and McWilliams, M., 1998, New ages for the climactic eruptions at Yellowstone: single crystal $^{40}Ar/^{39}Ar$ dating identified contamination: Geology, v. 26, p. 343–346, doi:10.1130/0091-7613(1998)026<0343:NAFTCE>2.3.CO;2.

Gradstein, F., Ogg, J., Schmitz, M., and Ogg, G., eds., 2012, The geologic time scale 2012: San Francisco, California, Elsevier, 1144 p., doi:10.1016/B978-0-444-59425-9.01001-5.

Hofmann, A.E., Valley, J.W., Watson, E.B., Cavosie, A.J., and Eiler, J.M., 2009, Sub-micron scale distributions of trace elements in zircon: Contributions to Mineralogy and Petrology, v. 158, p. 317–335, doi:10.1007/s00410-009-0385-6.

Horng, C.S., Lee, M.Y., Pälike, H., Wei, K.Y., Liang, W.T., Iizuka, Y., and Torii, M., 2002, Astronomically calibrated ages for geomagnetic reversals within the Matuyama chron: Earth, Planets, and Space, v. 54, p. 679–690.

Humphreys, E.D., Dueker, K.G., Schutt, D.L., and Smith, R.B., 2000, Beneath Yellowstone: Evaluating plume and nonplume models using teleseismic images of the upper mantle: GSA Today, v. 10, no. 12, p. 1–7.

James, D.E., Fouch, M.J., Carlson, R.W., and Roth, J.B., 2011, Slab fragmentation, edge flow and the origin of the Yellowstone hotspot track: Earth and Planetary Science Letters, v. 311, p. 124–135, doi:10.1016/j.epsl.2011.09.007.

Kuiper, K.F., Deino, A., Hilgen, F.J., Krijgsman, W., Renne, P.R., and Wijbrans, J.R., 2008, Synchronizing rock clocks of Earth history: Science, v. 320, p. 500–504, doi:10.1126/science.1154339.

Lanphere, M.A., Champion, D.E., Christiansen, R.L., Izett, G.A., and Obradovich, J.D., 2002, Revised ages for tuffs of the Yellowstone Plateau volcanic field: Assignment of the Huckleberry Ridge Tuff to a new geomagnetic polarity event: Geological Society of America Bulletin, v. 114, p. 559–568, doi:10.1130/0016-7606(2002)114<0559:RAFTOT>2.0.CO;2.

Miller, J., Matzel, J., Miller, C., Burgess, S., and Miller, R., 2007, Zircon growth and recycling during the assembly of large, composite arc plutons: Journal of Volcanology and Geothermal Research, v. 167, p. 282–299, doi:10.1016/j.jvolgeores.2007.04.019.

Obradovich, J.D., 1992, Geochronology of the late Cenozoic volcanism of Yellowstone National Park and adjoining areas, Wyoming and Idaho: U.S. Geological Survey Open-File Report 92-408, 45 p.

Pierce, K.L., and Morgan, L.A., 2009, Is the track of the Yellowstone hotspot driven by a deep mantle plume? Review of volcanism, faulting, and uplift in light of new data: Journal of Volcanology and Geothermal Research, v. 188, p. 1–25, doi:10.1016/j.jvolgeores.2009.07.009.

Quidelleur, X., Holt, J.W., Salvany, T., and Bouquerel, H., 2010, New K-Ar ages from La Montagne massif, Réunion Island (Indian Ocean), supporting two geomagnetic events in the time period 2.2–2.0 Ma: Geophysical Journal International, v. 182, p. 699–710, doi:10.1111/j.1365-246X.2010.04651.x.

Reynolds, R.L., 1977, Paleomagnetism of welded tuffs of the Yellowstone Group: Journal of Geophysical Research, v. 82, p. 3677–3693, doi:10.1029/JB082i026p03677.

Rivera, T.A., Storey, M., Zeeden, C., Hilgen, F.J., and Kuiper, K., 2011, A refined astronomically calibrated $^{40}Ar/^{39}Ar$ age for Fish Canyon sanidine: Earth and Planetary Science Letters, v. 311, p. 420–426, doi:10.1016/j.epsl.2011.09.017.

Rivera, T.A., Storey, M., Schmitz, M.D., and Crowley, J.L., 2013, Age intercalibration of $^{40}Ar/^{39}Ar$ sanidine and chemically distinct U/Pb zircon populations from the Alder Creek Rhyolite Quaternary geochronology standard: Chemical Geology, v. 345, p. 87–98, doi:10.1016/j.chemgeo.2013.02.021.

Sambridge, M.S., and Compston, W., 1994, Mixture modeling of multi-component data sets with application to ion-probe zircon ages: Earth and Planetary Science Letters, v. 128, p. 373–390, doi:10.1016/0012-821X(94)90157-0.

Singer, B.S., 2014, A Quaternary geomagnetic instability time scale: Quaternary Geochronology, v. 21, p. 29–52.

Vazquez, J.A., Kyriazis, S.F., Reid, M.R., Sehler, R.C., and Ramos, F.C., 2009, Thermochemical evolution of young rhyolites at Yellowstone: Evidence for a cooling by periodically replenished postcaldera magma reservoir: Journal of Volcanology and Geothermal Research, v. 188, p. 186–196, doi:10.1016/j.jvolgeores.2008.11.030.

Watson, E.B., and Harrison, T.M., 2005, Zircon thermometer reveals minimum melting conditions on earliest Earth: Science, v. 308, p. 841–844, doi:10.1126/science.1110873.